JOURNAL OF SPACECRAFT AND ROCKETS
Vol. 41, No. 4, July–August 2004

Electromagnetic Formation Flight for Multisatellite Arrays

Edmund M. C. Kong,* Daniel W. Kwon,† Samuel A. Schweighart,† Laila M. Elias,‡
Raymond J. Sedwick,§ and David W. Miller¶
Massachusetts Institute of Technology, Cambridge, Massachusetts 02139

The use of propellant to maintain the relative orientation of multiple spacecraft in a sparse aperture telescope such as NASA's Terrestrial Planet Finder (TPF) poses several issues. These include fuel depletion, optical contamination, plume impingement, thermal emission, and vibration excitation. An alternative is to eliminate the need for propellant, except for orbit transfer, and replace it with electromagnetic control. Relative separation, relative attitude, and inertial rotation of the array can all be controlled by creating electromagnetic dipoles on each spacecraft, in concert with reaction wheels, and varying their strengths and orientations. Whereas this does not require the existence of any naturally occurring magnetic fields, such as the Earth's, such fields can be exploited. Optimized designs are discussed for a generic system and a feasible design is shown to exist for a five-spacecraft, 75-m baseline TPF interferometer.

Nomenclature

A_c	=	conductor cross-sectional area
a	=	coil radius
c	=	conductor current density
c_0	=	constant defined in Eq. (8)
i	=	current
J	=	mission efficiency metric
l_c	=	conductor length
m_{coil}	=	electromagnetic coil mass
m_{em}	=	electromagnetic mass
m_{sa}	=	solar array mass
m_{sys}	=	total system mass
m_{tot}	=	total spacecraft mass
m_0	=	core bus and payload mass
n	=	number of coil turns
P	=	power
P_w	=	solar array specific power
p_c	=	conductor resistivity
R	=	resistance
r	=	conductor radius
s	=	array baseline
$\ddot{x}$	=	spacecraft acceleration
γ	=	mass fraction of total electromagnetic mass
η	=	amp turns
μ_0	=	permeability of free space
ρ	=	coil density
Σ	=	relative mission efficiency
ω	=	rotation rate

Received 29 April 2003; revision received 17 June 2003; accepted for publication 20 June 2003.

*Research Scientist, Department of Aeronautics and Astronautics, Room 37-471, 77 Massachusetts Avenue. Member AIAA.

†Graduate Research Assistant, Department of Aeronautics and Astronautics, Room 37-344a, 77 Massachusetts Avenue. Student Member AIAA.

‡Graduate Research Assistant, Department of Aeronautics and Astronautics, Room 37-354, 77 Massachusetts Avenue. Student Member AIAA.

§Principal Research Scientist, Department of Aeronautics and Astronautics, Room 37-431, 77 Massachusetts Avenue. Senior Member AIAA.

¶Professor, Department of Aeronautics and Astronautics; Director, Space Systems Laboratory, Room 37-327, 77 Massachusetts Avenue. Senior Member AIAA.

Introduction

A NUMBER of NASA missions are considering multiple spacecraft architectures for a variety of reasons. First, multiple spacecraft can be separated to large baselines, thereby improving angular resolution for imaging, astrometry, planet detection, and characterization. Second, each spacecraft in the formation can be smaller than a single spacecraft designed to perform the same mission and, thereby, provide easier packaging, launch, and deployment. Third, because interspacecraft interfaces are soft, for example, communications, optics, control, metrology, if a spacecraft fails, it can easily be removed from the formation and replaced with a functioning spacecraft. Fourth, as technology improves, replacement spacecraft can be launched and integrated into the array thereby evolving the formation's capabilities without the costly block changes typical of past programs.

Although these benefits are clear, there are several drawbacks. For example, precision formation flight of the satellites in the array requires that propellant be expended to maintain the formation geometry. This has several implications. First, propellant is a consumable, which, once depleted, renders the satellite useless. Second, the impingement of a thruster plume on a neighboring spacecraft can cause a dynamic disturbance to its stability, deposit particulates on sensitive optics, induce inadvertent charging, and actually ablate material off the spacecraft, thereby causing permanent damage. Third, for missions such as NASA's Terrestrial Planet Finder (TPF), the propellant plume can put a thermally bright haze across the line of sight of the telescope. For example, micrometer particles at room temperature can blind TPF even if the particles are many kilometers away.[1] Furthermore, low-speed plume exhaust will tend to orbit near the spacecraft creating a local pollution haze through which the telescope must look.

As one explores the design of these systems in more depth, one recognizes that there is a mismatch between the geometric requirements that the formation must achieve and the way in which that geometry is controlled. Specifically, the relative separations between spacecraft, not the absolute positions in space, are important. However, thrusters actuate absolute degrees of freedom, which necessitates the use of a consumable. Therefore, it would be desirable if a form of formation control could be developed that does not rely on consumables and reduces the amount of contamination that is introduced by thrusters.

The Massachusetts Institute of Technology (MIT) Space Systems Laboratory's Electromagnetic Formation Flight (EMFF) program seeks to develop multiple satellite formation control strategies that exploit electromagnetic forces between spacecraft to control formation geometry. EMFF controls relative positions and orientations between spacecraft through the use of a renewable energy source: electrical power. Dipole topologies allow an increasing variety of relative

degrees of freedom between spacecraft to be controlled without the expenditure of propellant. For this paper, the use of electromagnetic dipoles for relative position and orientation maintenance as needed for TPF will be addressed.

Maximizing Mission Efficiency

The objective of this section is to derive the fundamental relations for optimizing the mission efficiency of rotating separated spacecraft interferometers using electromagnets. The measure of mission efficiency is science productivity divided by mission cost. In this paper, science productivity is defined as rotation rate because the faster an interferometric version of the TPF telescope can rotate, the quicker it can survey the region around a potential terrestrial planet-supporting star and, therefore, the more stars it can survey in a given amount of time. Of course, once this rotation rate becomes high enough, photon starvation will limit the achievable rotation rate due to the need to achieve a certain signal-to-noise ratio at each rotation angle. Cost is crudely defined as system mass because launch costs increase as the mass of the system increases. The productivity per cost is improved when either rotation rate is increased or mass is reduced. Maximizing mission efficiency (MME) entails calculating required mass, generated force, and the resulting rotation rate.

Two-Spacecraft Case

The geometry of a two-spacecraft example is shown in Fig. 1. Each spacecraft contains an electromagnetic coil of diameter $2a$, and the spacecraft are separated by a baseline s. The longitudinal axes of the two coils are collinear. The two spacecraft orbit about their common center with an angular rate of ω, and the requisite centripetal acceleration is provided by the electromagnetic attraction between the spacecraft caused by inducing currents in the coils. In this two-spacecraft example, both spacecraft and both coils are identical.

The total spacecraft mass is composed of the core bus and payload, the electromagnetic coil, and the solar array:

$$m_{\text{tot}} = m_0 + m_{\text{coil}} + m_{\text{sa}} \tag{1}$$

Obviously, other mass elements can be included to account for other power subsystem elements, etc. However, the mass elements modeled here do capture at the coarsest level the trades between coil size and consumed power.

The mass of the coil equals its density times its volume (conductor length times cross-sectional area), which, in turn, depends on coil radius, conductor radius, and number of turns in the coil:

$$m_{\text{coil}} = l_c A_c \rho_c = (2\pi an)(\pi r^2)\rho_c = 2(\pi r)^2 na\rho_c \tag{2}$$

The solar array mass equals power divided by specific power, or watts generated per kilogram of solar array:

$$m_{\text{sa}} = P/P_W = i^2 R \big/ P_W = i^2 \big/ P_W (p_c l_c / A_c)$$

$$= \left(i^2 \big/ P_W\right) p_c (2\pi an/\pi r^2) = 2(i/r)^2 p_c an / P_W \tag{3}$$

Power depends on resistance, which, in turn, is dependent on conductor resistivity and conductor geometry.

Now that total mass and, therefore, cost is modeled, the generated force can be used to derive rotation rate and, therefore, productivity. The generated force is a function of permeability, coil geometry, and vehicle separation and, assuming two ideal dipoles in the far field, is given by

$$F = \tfrac{3}{2}\mu_0 \pi (n^2 i^2 a^4 / s^4) \tag{4}$$

Equating to the centripetal force needed for circular motion allows the rotation rate to be found:

$$\omega = \sqrt{3\mu_0 \pi \big/ s^5}\, nia^2 \big/ \sqrt{m_{\text{tot}}} \tag{5}$$

As expected, increasing mass and separation distance reduces rotation rate while increasing amp turns (ni), and the area enclosed by the coil increases rotation rate.

When a mission efficiency metric is defined as one that divides rotation rate by total system mass, increasing coil and solar array masses drive the metric downward, whereas increasing rotation rate drives the metric up:

$$J = \omega / c_0 m_{\text{sys}} = \omega / c_0 2m_{\text{tot}} = nia^2 \big/ 2m_{\text{tot}}^{\frac{3}{2}} \tag{6}$$

where

$$m_{\text{sys}} = 2m_{\text{tot}} \tag{7}$$

$$c_0 = \sqrt{3\mu_0 \pi \big/ s^5} \tag{8}$$

Maximize the metric with respect to the number of turns in the coil:

$$\frac{\partial J}{\partial n} = 0 \Rightarrow n_{\text{opt}} = \frac{m_0}{a\left[\pi^2 \rho_c r^2 + \left(i^2 p_c \big/ P_W r^2\right)\right]} \tag{9}$$

As expected, more coil turns are needed for more massive payloads and core buses, whereas fewer coil turns are needed as coil diameter increases. This relationship for the optimum number of turns can then be used to update the total mass:

$$m_{\text{tot}}|_{n_{\text{opt}}} = 3m_0 \tag{10}$$

This is a surprisingly simple result that states that the optimum total mass of the spacecraft is simply a function of the payload and associated bus mass. The mission efficiency metric can also be updated giving

$$J|_{n_{\text{opt}}} = \frac{1}{2\sqrt{27m_0}} \frac{ia}{\pi^2 \rho_c r^2 + \left(i^2 p_c \big/ P_W r^2\right)} \tag{11}$$

Maximizing this updated metric with respect to current in the coil results in an optimum value for current:

$$\frac{\partial J}{\partial i} = 0 \Rightarrow i_{\text{opt}} = \pi r^2 \sqrt{P_W \frac{\rho_c}{p_c}} \tag{12}$$

As expected, the optimum current increases with conductor radius, specific power of the solar array, and density but decreases with increasing resistivity. Updating the mission efficiency with the optimum coil current gives

$$J|_{i_{\text{opt}}} = a \big/ 4\pi \sqrt{27m_0} \sqrt{P_W / \rho_c p_c} \tag{13}$$

where mission efficiency degrades with bus and payload mass, coil density, and resistivity but increases with coil diameter and solar array specific power. While the maximum efficiency depends on payload, solar array, and conductor properties, which are likely fixed by current technology, it is proportional to coil radius. The larger the coil, the more area it encloses and the more efficient the design. Obviously, the need to mount and support large coils will eventually place an upper limit on achievable coil geometry.

The updated optimum number of coil turns is now

$$n_{\text{opt}} = m_0 \big/ 2\pi^2 a \rho_c r^2 \tag{14}$$

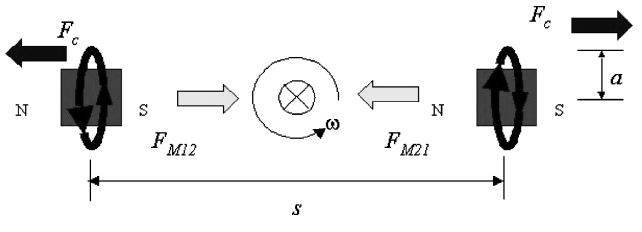

Fig. 1 Geometry of two-spacecraft case.

Notice that the optimum coil turns is inversely proportional to conductor radius squared, whereas the optimum coil current is proportional to conductor radius squared. As a result, the important design parameter is actually amp turns, and conductor radius simply determines whether the requisite amp turns are achieved mostly through current or turns. The optimum amp turns is given by

$$ni|_{\text{opt}} = m_0/2\pi a\sqrt{P_W/\rho_c p_c} \tag{15}$$

This result states that the optimum value for amp turns increases with payload mass and solar array specific power but decreases with coil size and conductor properties.

This has been an interesting exercise in that it has revealed that there are clearly preferable designs within the design trade space. It has been confirmed that all optima [Eqs. (9) and (12)] correspond to maxima. However, it has only captured a few of the most important design issues. The following sections expand on this analysis to include additional spacecraft, as well as high-temperature superconducting coils.

Adding a Combiner Spacecraft

Optical interferometry requires that a combiner system be placed at an equal optical pathlength location. In this example, that location will be assumed to be at the center of rotation. This requires the addition of a third, combiner spacecraft. Therefore, assume all satellites are identical and that a third identical satellite is placed at the center of rotation. Now, summing the forces on a collector spacecraft and equating that to the requisite centripetal force gives

$$\frac{3}{2}\mu_0\pi n^2 i^2 a^4\left(\frac{1}{(s/2)^4}+\frac{1}{s^4}\right) = \frac{1}{2}m_{\text{tot}}\omega^2 s \tag{16}$$

where the two terms in parentheses confirm that two spacecraft exert attractive forces on the third, although the force from the other collector spacecraft is only 1/16th the force from the combiner. Now the efficiency metric for three spacecraft is

$$J_3 = \omega/c_0 m_{\text{sys}} = \omega/c_0 3m_{\text{tot}} = \sqrt{17}\Big/3\left(nia^2\Big/m_{\text{tot}}^{\frac{3}{2}}\right) \tag{17}$$

Notice that this expression for three-spacecraft mission efficiency is identical to that for two spacecraft with the exception of the numerical constant. Therefore, the optimization process, with respect to the design parameters, is identical, yielding the same optimum values. As a result, the relative efficiency between the three- and two-spacecraft arrays can be found by dividing Eq. (17) by Eq. (6) to give

$$\Sigma_3 = \frac{J_3}{J_2} = \frac{\sqrt{17}\left(nia^2\Big/3m_{\text{tot}}^{\frac{3}{2}}\right)}{nia^2\Big/2m_{\text{tot}}^{\frac{3}{2}}} = \frac{2}{3}\sqrt{17} = 2.75 \tag{18}$$

Adding a combiner almost triples the mission efficiency due to the placement of an identical spacecraft at the midpoint of the two-spacecraft array and, thereby, inserting an electromagnet into the system that exerts a force on the collector spacecraft that is 16 times that exerted by the other collector.

Additional Spacecraft

Uniformly incrementing the array with additional identical spacecraft will continue the trend of increasing the mission efficiency. For N identical spacecraft in a uniformly separated array, the efficiency metric J_N can be determined by

$$J_N = \sqrt{\sum_{i=1}^{N-1}\left(\frac{N-1}{i}\right)^4}\Bigg/N\frac{nia^2}{m_{\text{tot}}^{\frac{3}{2}}} \tag{19}$$

Results of the optimized design parameters for two spacecraft and N spacecraft are summarized in Table 1. The relative efficiency between N spacecraft and $N-1$ spacecraft for systems with more than two spacecraft is

$$\Sigma_N = \frac{J_N}{J_{N-1}} = \frac{N-1}{N}\left[\sqrt{\sum_{i=1}^{N-1}\left(\frac{N-1}{i}\right)^4}\Bigg/\sqrt{\sum_{i=1}^{N-2}\left(\frac{N-2}{i}\right)^4}\right]$$

$$= \frac{(N-1)^3}{N(N-2)^2}\sqrt{1+\left[1\Big/(N-1)^4\sum_{i=1}^{N-2}\frac{1}{i^4}\right]}, \qquad N>2 \tag{20}$$

Although additional spacecraft will increase J, there are diminishing returns in relative efficiency. For example, a five-spacecraft array has a 40% improvement in mission efficiency over a four-spacecraft array; however, a six-spacecraft array over a five-spacecraft array only has a 25% improvement in mission efficiency. This trend continues, and for large N, Σ_N approaches 1.

Table 1 Optimized design parameters for a two spacecraft array

Parameter	Two-spacecraft case	N-spacecraft case
	Coil	
Turns	$n_{\text{opt}} = \dfrac{m_0}{2\pi^2 a\rho_c r^2}$	$n_{\text{opt}} = \dfrac{m_0}{2\pi^2 a\rho_c r^2}$
Current	$i_{\text{opt}} = \pi r^2\sqrt{\dfrac{P_W\rho_c}{p_c}}$	$i_{\text{opt}} = \pi r^2\sqrt{\dfrac{P_W\rho_c}{p_c}}$
Amp turns	$ni\|_{\text{opt}} = \dfrac{m_0}{2\pi a}\sqrt{\dfrac{P_W}{\rho_c p_c}}$	$ni\|_{\text{opt}} = \dfrac{m_0}{2\pi a}\sqrt{\dfrac{P_W}{\rho_c p_c}}$
	Spacecraft	
Mass	$m_{\text{opt}} = 3m_0$	$m_{\text{opt}} = 3m_0$
Power	$P_{\text{opt}} = m_0 P_W$	$P_{\text{opt}} = m_0 P_W$
Rotation rate	$\omega_{\text{opt}} = \sqrt{\dfrac{3\mu_0\pi}{B^5}}\dfrac{a\sqrt{m_0}}{2\sqrt{3}\pi}\sqrt{\dfrac{P_W}{\rho_c p_c}}$	$\omega_{\text{opt}} = \sqrt{\sum_{i=1}^{N-1}\left(\dfrac{N-1}{i}\right)^4}\sqrt{\dfrac{3\mu_0\pi}{B^5}}\dfrac{a\sqrt{m_0}}{2\sqrt{3}\pi}\sqrt{\dfrac{P_W}{\rho_c p_c}}$
	System	
Mass	$m_{\text{sys}} = 6m_0$	$m_{\text{sys}} = 3Nm_0$
Efficiency	$J_{\text{opt}} = \dfrac{a}{4\pi\sqrt{27m_0}}\sqrt{\dfrac{P_W}{\rho_c p_c}}$	$J_{\text{opt}} = \sqrt{\sum_{i=1}^{N}\left(\dfrac{N-1}{i}\right)^4}\Bigg/N\dfrac{a}{2\pi\sqrt{27m_0}}\sqrt{\dfrac{P_W}{\rho_c p_c}}$

Nonidentical Configuration

The MME design of an array applies very well with spacecraft of equal masses and for rotating systems. Instead of using ω as a critical design factor, a more generalized design parameter is the spacecraft agility, or acceleration of a spacecraft or array. Now, given design restrictions on total mass, the mass of an array can be distributed to optimize its acceleration. Similar to ω, the acceleration of a spacecraft determines its productivity. In a three-spacecraft array, the center spacecraft may consist of different number of amp turns η_i from that of the two outer spacecraft η_0, while it is assumed that the coil diameters are identical. The generated force is similar to that of Eq. (4) and can be solved for the acceleration of the outer spacecraft of the array, where η is substituted for amp-turns product ni:

$$\ddot{x}_0 = \tfrac{3}{2}\mu_0\pi\left(a^4 \Big/ m_{0_{\text{total}}} s^4\right)\left(16\eta_i\eta_0 + \eta_0^2\right) \tag{21}$$

$$\eta = ni \tag{22}$$

The electromagnetic mass of a spacecraft consists of the coil mass and solar array mass. To simplify the approach, the coil and solar array masses [Eq. (2) and (3)] have been rewritten in terms of the current density of the conductor:

$$\begin{aligned} m_{\text{em}} &= m_{\text{coil}} + m_{\text{sa}} = 2(\pi r)^2 na\rho_c + 2(i/r)^2 p_c an/P_w \\ &= 2\pi nia(\rho_c/c) + 2\pi nia(p_c c/P_w) \\ &= 2\pi\eta a[(\rho_c/c) + (p_c c/P_w)] \end{aligned} \tag{23}$$

The total mass of each spacecraft [Eq. (1)] can now be redefined as

$$m_{\text{total}} = m_0 + m_{\text{em}} = m_0 + 2\pi\eta a\beta \tag{24}$$

where

$$\beta = (\rho_c/c) + (p_c c/P_w) \tag{25}$$

The three-spacecraft array consists of two layers. The inner layer consists of the center spacecraft bus and payload mass and the electromagnetic mass, and the outer layer consists of the two identical bus and payload masses and the electromagnetic mass of the outer spacecraft. The bus and payload mass of each spacecraft is assumed to be equal because they will have similar payloads for optics, avionics, etc. Therefore, the electromagnetic mass will be optimally distributed according to a mass fraction of the total electromagnetic mass:

$$m_{\text{em}_i} = \gamma m_{\text{em}_{\text{total}}} \tag{26}$$

$$m_{\text{em}_0} = [(1-\gamma)/2]m_{\text{em}_{\text{total}}} \tag{27}$$

This can be used with Eq. (24) to solve for the amp turns for each layer:

$$\eta_0 = [(1-\gamma)/2]m_{\text{em}_{\text{total}}} \Big/ 2\pi a\beta \tag{28}$$

$$\eta_i = \gamma\left(m_{\text{em}_{\text{total}}} \Big/ 2\pi a\beta\right) \tag{29}$$

When this result is used, the acceleration of the array from Eq. (21) can be defined in terms of γ. Maximize with respect to the mass fraction, the optimal mass fraction is found to be a function of bus and payload mass and total electromagnetic (EM) mass:

$$\frac{\partial\ddot{x}}{\partial\gamma} = 0 \Rightarrow \gamma_{\text{opt}} = \frac{62m_0 + 31m_{\text{em}} - 2\sqrt{31m_0}\sqrt{31m_0 + 16m_{\text{em}}}}{31m_{\text{em}}} \tag{30}$$

For a spacecraft with a dry mass of 600 kg, similar to that of a TPF collector (Table 2), the optimal mass fraction of a three-spacecraft array is shown in Fig. 2. The optimum mass fraction is far from the identical three-spacecraft configuration with close to half the total EM mass located on the center spacecraft. This is because the center spacecraft does not need to translate relative to the other spacecraft. However, some EM mass is needed on each spacecraft because the centripetal force is created by their mutual interaction. Therefore, there is no mass penalty on the center spacecraft and the resulting EM mass is much greater than that of the outer spacecraft.

Table 2 TPF spacecraft mass breakdown[1]

	Collector spacecraft		Combiner spacecraft	
Mass component	Mass, kg	Power, W	Mass, kg	Power, W
Dry	600	268	568	687
Propulsion	96	300	96	300
Propellant	35	N/A	23	N/A

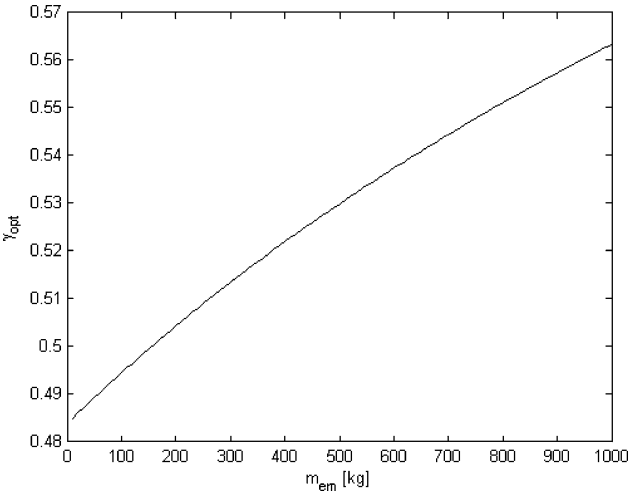

Fig. 2 Optimal EM mass fraction of the center spacecraft for three-spacecraft array with 600-kg dry mass.

Spacecraft with Superconducting Coils

To generate large magnetic dipoles, high-current EM coils with many turns and high-power requirements must be used. This, however, drives up EM coil and solar array masses. Conventional coil conductors such as copper suffer from such high-current application because resistance causes significant heat generation and power losses. Therefore, the design should utilize a coil that has the lowest resistance possible.

Superconducting material has zero resistance when cooled below a critical temperature, resulting in no thermal heating and no power losses across the wire. With high-temperature superconducting (HTS) wire, an electromagnet could be built to any size needed. Because there is no resistance, there is no heat production, and a coil of any cross-sectional area can be made without fear of overheating the wire. Zero resistance also means no power is required to produce a high current through the wire, causing the mass of the solar array to be determined by the power requirements of the spacecraft bus and payload mass and not the coil. The only losses are in the power subsystem itself such as from regulators, switches, and batteries. Therefore, the only limitation on the current is the critical current density of the superconducting wire.

Case Study: TPF

The analysis performed in the preceding section is now extended to the five-spacecraft TPF interferometer. The relative positions of the spacecraft are shown in Fig. 3. The maximum baseline for the TPF interferometer is currently envisioned to be at 75 m and rotated at one rotation every 2 h. In this section, mission parameters specific to the TPF interferometer are first presented. The best design based on these parameters is then determined. In the next section, the design obtained here is compared to currently proposed propulsion systems for TPF.

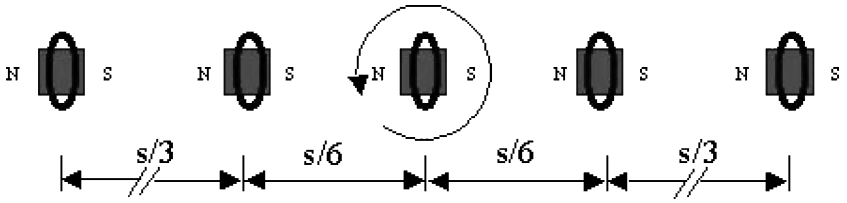

Fig. 3 Five-spacecraft EMFF TPF interferometer.

TPF Spacecraft Dry Mass

The dry mass of the spacecraft is obtained based on the total spacecraft mass from the TPF book.[1] To fairly compare the various systems, the dry mass of the spacecraft will exclude not only the propellant mass allocated for the TPF mission, but the propulsion system and the solar array mass that are associated with it. The breakdown of both the combiner and collector spacecraft masses, together with the budgeted power, is shown in Table 2.

Coil Properties

Coil designs using room temperature copper coils and HTS wire were conducted. Copper coils were used to determine a preliminary design and obtain order of magnitude results. HTS wire was used because the strengths of the magnetic attraction between the spacecraft are proportional to the product of the currents in the conducting coils [Eqs. (4), (16), and (19)]. As such, to maximize the magnetic dipole strength and minimize the power required, conducting coils made out of HTS material are quite suitable. The density of the HTS wire is approximately 13,608 $\mathrm{kg}\cdot\mathrm{m}^{-3}$. This was determined from a 1.3608-kg $100 \times 0.004 \times 0.00025$ m^3 sample of HTS wire obtained from American Superconductor.**

Solar Array

The power required for this EMFF concept is assumed to be generated entirely from the solar arrays. In this study, a conversion factor of 25 W/kg from the power required to the corresponding solar array mass[2] is used.

MME Design

The MME design approach outlined in the preceding section is now extended to the five-spacecraft TPF interferometer. To simplify the problem, the EM coil design for all of the spacecraft is made the same. When symmetry is assumed, the kinetic constraints that must be satisfied by the two collector spacecraft rotating about the combiner are, therefore,

$$m_{\mathrm{sc1}} s\omega^2/2 = \tfrac{3}{2}\mu_0 \pi n^2 a^4 i_1 \left\{ \left[i_2/(s/3)^4 \right] + \left[i_3/(s/2)^4 \right] + \left[i_2/(2s/3)^4 \right] + \left(i_1/s^4 \right) \right\} \tag{31}$$

$$m_{\mathrm{sc2}} s\omega^2/6 = \tfrac{3}{2}\mu_0 \pi n^2 a^4 i_2 \left\{ -\left[i_1/(s/3)^4 \right] + \left[i_3/(s/6)^4 \right] + \left[i_2/(s/3)^4 \right] + \left[i_1/(2s/3)^4 \right] \right\} \tag{32}$$

which clearly shows the EM force interaction between these spacecraft and all of the others in the interferometer. Note that the rotational rate ω in both of these equations is in fact the same. When these two equations are equated to eliminate ω, an expression for the current in the combiner spacecraft, i_3, can be determined. When either Eq. (31) or Eq. (32) is divided with the total mass of interferometer and the expression for i_3 is substituted, the mission efficiency metric for this system is then a function of the radius of the coil, a, the number of conductor turns, n, the radius of the conductor, r, the current in outermost collector, i_1, and the current in the inner collector, i_2:

$$J_{\mathrm{MME}} = \omega/m_{\mathrm{tot}} = f(a, n, r, i_1, i_2) \tag{33}$$

**Data available online at "High Current Density Wire," URL: http://www.amsuper.com [cited 2 February 2003].

Table 3 MME design for TPF configuration

Parameter	Spacecraft 1	Spacecraft 2	Spacecraft 3	Total array
a, m	10	10	10	——
n, turns	313	313	313	——
r, mm	1	1	1	——
Current, A	11.4469	0.0353	24.0178	——
Power, W	1.27×10^4	0.123	5.61×10^4	——
m_{sc}, kg	1714	1204.3	3416.1	9252.7
ω, rad/s	0.0036	0.0036	0.0036	0.0036
$J = \omega/m_{\mathrm{tot}}$	——	——	——	3.90×10^{-7}
F_{cent}, N	0.8358	0.1958	——	——

In the ideal situation, the optimal design using this mission efficiency metric can be determined by simply taking the first derivative of Eq. (33) with respect to one of the five variables and setting it to zero to obtain the optimal design for that variable. This optimal variable can then be substituted back into Eq. (33), which makes it dependent on only the remaining four variables. This process can then be repeated until all five variables are determined in terms of all of the other known parameters. Unfortunately, as the number of spacecraft in the array increases, the determination of the optimal solution analytically is no longer practical. One, however, can resort to numerical optimization techniques.

When the fmincon optimization routine in the MATLAB® numerical package[3] is used, the maximum mission efficiency design obtained is tabulated in Table 3. The dimensions of the coil in this design seem to be reasonable in that they are not excessively large. However, these dimensions do translate to a rather massive system when compared to the dry mass of the spacecraft. The current and power levels are rather high, especially for the combiner spacecraft. The rotation rate of the interferometer is large as well (0.0036 rad/s), especially when compared to the TPF rotation rate of 8.73×10^{-4} rad/s. As for the inner combiner spacecraft, little power is required for this spacecraft, and the combiner and outer collector spacecraft provide most of the EM forces. Even though this design maximizes the mission efficiency, the interferometer may be rotating too fast for the system to collect enough photons to detect a planet in the extrasolar system. Also, significant control issues must also be considered when such a massive system is rotated quickly.

As such, in the next subsection, this optimization is repeated with the rotation rate of the interferometer specified. The mission efficiency metric, in this case, is reduced to a mass minimization metric where the kinetic constraints [Eqs. (31) and (32)] must again be satisfied.

Fixed Rotation Designs

The optimal designs for a range of interferometer rotation rates ω are determined. The approach here is similar to the one in the preceding subsection. First, the current in the combiner spacecraft, i_3, is found by equating the two kinetic equations (31) and (32). Then, with the rotation rate being specified, an explicit expression for the current in the inner collector spacecraft, i_2, is determined from one of the two kinetic equations. When these two current expressions are substituted for, the total mass of the interferometer can be expressed as a function of the following four variables:

$$m_{\mathrm{tot}} = f(a, n, r, i_1) \tag{34}$$

as opposed to the five in the preceding subsection.

Table 4 Superconducting EMFF design for TPF interferometer

Power, W	n, turns	Current, A	a, m	A_c, mm^2	m_{sc}, kg	$F_{on\ 1}$, mN	$F_{on\ 2}$, mN
400	113	71.4	2	1	627.49	$F_{cent} = -17.92$	$F_{21} = -16.64$
400	119	71.4	2	1	628.51	$F_{12} = 16.64$	$F_{cent} = -5.89$
400	2	71.4	2	1	576.46	$F_{13} = 0.06$	$F_{23} = 4.71$
400	119	71.4	2	1	628.51	$F_{14} = 1.04$	$F_{24} = 17.52$
400	113	71.4	2	1	627.49	$F_{15} = 0.20$	$F_{25} = 1.04$

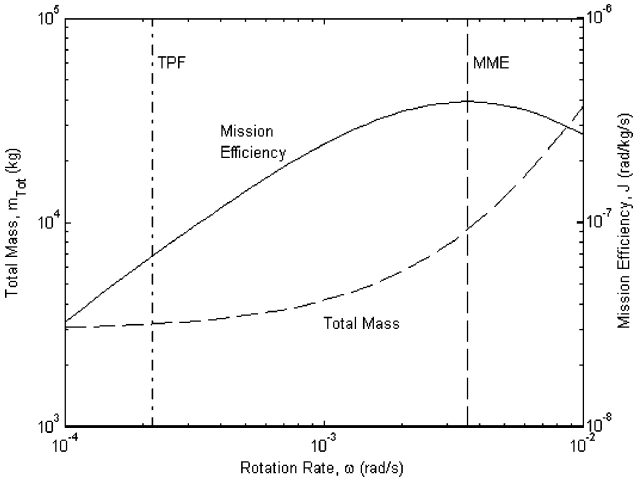

Fig. 4 Interferometer mass and mission efficiency as a function of rotation rate.

Again, the best designs for the various rotation rates are determined using the fmincon optimization routine in MATLAB with the results plotted in Fig. 4. For interferometers that are rotating at a low angular rate, the required EM masses are low. As the rotation rate is increased, larger coils are needed to balance the higher centripetal load experienced by the collector spacecraft. The corresponding mission efficiencies are also shown in Fig. 4. Observed is the existence of an optimum, where the mission efficiency of the system can no longer be improved. Clearly the preference is to operate the interferometer near this optimum if the rotation rate or the total mass is not subjected to any constraints. However, if these constraints exist, the achievable mission efficiency can then be determined together with either the corresponding minimum total mass or maximum rotation rate that is to be expected. The optimum shown in Fig. 4 does in fact correspond to the MME design obtained in the preceding subsection.

Also shown in Fig. 4 is the best TPF design based on a rotation rate of one rotation every 2 h as currently proposed for TPF.[1] At this rate, the maximum achievable mission efficiency is 2.20×10^{-7} rad/kg $\cdot$ s compared with the MME design of 3.90×10^{-7} rad/kg $\cdot$ s, a 56% drop. However, this EM TPF design requires 1003 kg of additional EM mass (3971 kg total mass) compared with the extra 6285 kg of EM mass required for the MME design.

Even though the EM TPF design has a large EM mass savings (5282 kg) over the MME design, EM mass consists of approximately one-fourth of the spacecraft total mass. Significant mass savings can be achieved using HTS wire instead of room temperature copper coils. Table 4 shows the design parameters for a minimum mass superconducting EM TPF. The superconducting EM consists of only 3.9% of its total mass (3088.4 kg) and has a large mass savings (883 kg) over the copper coil design.

The first item shown in Table 4 is the power required for each of the spacecraft. The power levels required for each of the spacecraft was an estimate of the power needed for the core and bus masses because the superconducting coil required no power. The dimensions of the coil designs seem to be quite reasonable as well. Both the centripetal and magnetic forces acting on the two collector and combiner spacecraft are also shown in Table 4. For the outermost spacecraft, the centripetal loading on the spacecraft seems to be the highest. This tends to makes sense because this spacecraft is farthest away from the center of the array. To offset the centripetal load, the magnetic attraction to the second collector spacecraft is the highest because it is closest to it. The inner collector spacecraft, however, experiences a lower centripetal load with strong attraction between them. As opposed to the outermost spacecraft, this strong attraction force is primarily required to offset the attraction to the outermost spacecraft. A quick glance over the parameters shown in the superconducting design case seems to indicate that most of the attraction force to counteract the centripetal loading is generated by the collector spacecraft. The parameters that define the EM coil seem to be quite comparable and reasonable as well. The superconducting EM TPF design can easily be realizable and launched in either the extended expendable launch vehicle, Ariane 5, or VentureStar, all launch vehicles that are currently considered for the TPF interferometer. In the next section, the copper coil and superconducting EMFF designs are compared with the other propulsion options.

TPF Comparisons

A recent study at MIT compared the use of the following propulsion systems for the various NASA formation flight missions: cold gas thrusters; colloids, pulse plasma thrusters (PPTs), and field emission electrostatic propulsion thrusters (FEEPs).[4] The study compared the different micropropulsion systems for the purpose of station keeping by implementing them in representative control strategies to evaluate the propellant usage. The overall system mass and cost were compared and included an estimate of the cost of bringing each type of propulsion system from its current technology readiness level (TRL) up to TRL 8. For the purpose of station keeping, the study recommended the use of either PPTs or FEEPs for the TPF interferometer based on the cost to realize the propulsion system. In this section, the EMFF designs obtained in the preceding section are compared to formation flight designs that consider these propulsive options.

For the propellant-based options, the mass of each spacecraft can be broken into the dry mass of the spacecraft, m_{dry}, the mass of the propulsion system, $m_{propulsion}$, and the mass of the propellant, $m_{propellant}$. To ensure fair comparison of the overall mass for the various formation flight options, the mass of the solar array panel associated with the power required to operate the propulsion is also included. As such, the mass of each spacecraft in an array that utilizes a propulsion-based system is given by

$$m_{sc} = m_{dry} + m_{propulsion} + m_{propellant} + m_{sa} \tag{35}$$

The designs of the four micropropulsion systems considered in this study can be found by Reichbach et al.[4] In this study, only the results based on the analysis are presented with the EM formation flight option.

The overall mass performance for the TPF interferometer using the various formation flight options is shown in Fig. 5. For all of the propulsion-based systems, Fig. 5 clearly indicates increases in overall system mass as the mission lifetime is extended. To keep the array rotating, propellant is required to provide the centripetal loads that are needed by the respective spacecraft. The high propellant expenditure rates seem to rule out the use of the low specific impulse cold gas option, $I_{sp} = 65$ s. When higher specific impulse systems are used, less propellant is required; thus, these are more attractive options. However, when compared to the constant mass superconducting EM design, the FEEPs propulsion system becomes a less attractive option from a mass standpoint when a mission lifetime of approximately more than six years is considered. The mission duration of TPF is projected to be greater than five years.[1] As for

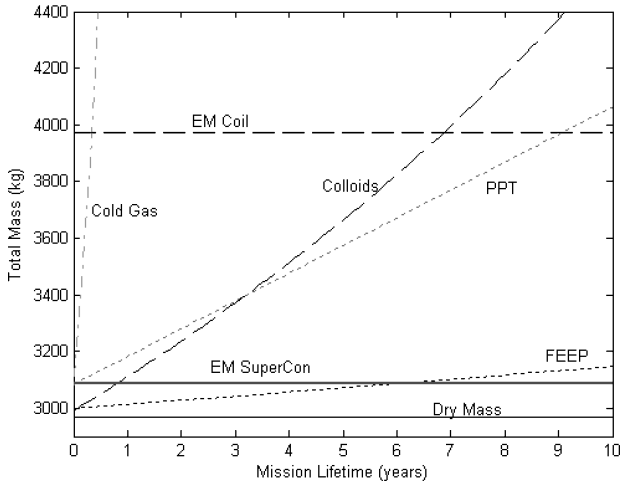

Fig. 5 Mass comparison for TPF using various propulsion systems (2-h rotation).

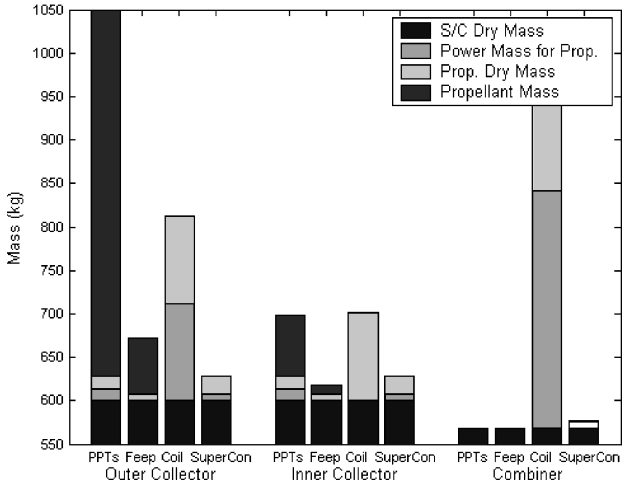

Fig. 6 Mass breakdown for various propulsion system ($T = 10$ years).

the crossover between the colloids and the PPTs, the increase in propellant mass for the colloid requires an equivalent increase in colloid feeding system and, thus, the overall propulsion mass. The low superconducting EM coil mass that is required for the EMFF option is clearly the most attractive.

The mass breakdown for the various formation flight options with a mission lifetime of 10 years is shown in Fig. 6. The breakdown across the different options is grouped in terms of the outer most collector spacecraft, the inner collector spacecraft, and the combiner spacecraft. Because the outermost spacecraft need the highest centripetal load, it is not surprising to see these spacecraft with the most mass in the array for the propulsive option. In both the propulsive options shown in Fig. 6, the spacecraft mass is clearly dominated by the propellant mass.

Relatively high spacecraft mass is also observed for the EM option with room temperature copper coils. Relatively large coils (10 m) are required to produce the desired magnetic force compared to the superconducting coils (2 m), which increase magnetic attraction significantly with little mass and power penalty. In contrast to the superconducting option, the copper coil design requires a large power mass, which is especially noticeable for the combiner spacecraft. The copper coil option is still more favorable for long-duration missions than the PPT and colloid options. Both EM options have either a large combiner or large inner collector spacecraft. This is because EM mass favors spacecraft closer to the center of the array because they experience less translation and, thus, have less of a mass penalty associated with adding EM mass. This result supports the nonidentical configuration analysis outlined earlier.

The only disadvantage observed in using superconducting EMFF is that it requires a higher combiner spacecraft mass when compared to the propulsive options. In this analysis, the propellant associated with rotating the combiner spacecraft has not been considered. In the case of the EM option, a magnetic force contribution from the combiner spacecraft is required. This magnetic force contribution, albeit small, requires that a coil design be included. This small mass differential is, however, easily offset by the large differential when the collector spacecraft are compared, thus making the superconducting EM design the most desirable.

Dynamics and Control

Finally, a brief discussion of the dynamics and controls issues of the EMFF architectures proposed in the preceding section is necessary to better understand the challenges and future work in this research. It can be intuitively seen (and rigorously shown) that the spinning spacecraft arrays considered in this paper are inherently unstable. Interaction forces between the electromagnets on each spacecraft provide the centripetal loads necessary to maintain a steady-state rotation of the array, and these forces are modulated to maintain precise spacecraft separation distances in the presence of disturbances. Clearly if these forces are slightly larger or smaller than necessary, the spacecraft will tend to approach one another or separate in an unstable manner. Hence, an investigation of the dynamics of such a system, including stability and controllability analyses, is vital to demonstrating the feasibility of the EMFF concept.

A simplified two-spacecraft EMFF system was shown by Elias et al.[5] to be dynamically unstable but stabilizable using closed-loop control. As discussed by Elias et al.,[5] a representative hardware system with unstable dynamics similar to a simplified two-spacecraft system was used to demonstrate closed-loop control and stable close-loop dynamics of a one-degree-of-freedom system.

Additionally, evidence will be presented in a forthcoming publication demonstrating that a full-degree-of-freedom, two-spacecraft EMFF system (with each spacecraft having three translational and three rotational degrees of freedom) is also dynamically unstable, with open-loop poles both in the closed left-half and right-half complex plane. However, this system can be stabilized using optimal control techniques if each spacecraft has at least three perpendicular EM actuators and three perpendicular reaction wheels. All of the closed-loop poles of the system then lie in the open left-half complex plane, and time simulations show the closed-loop dynamics to be stable. Hence the system dynamics, both within and perpendicular to the plane of rotation of the array, are stabilizable using closed-loop control.

One final dynamic consideration is the coupling of actuators in such an EMFF system. For example, when the attitude of one spacecraft in a two-spacecraft array is disturbed such that its primary electromagnet (providing the centripetal load) rotates away from the line of sight to the other spacecraft, unintended torques arise on both spacecraft. In this example, the torques tend to restore the desired attitude, despite causing oscillations of the degrees of freedom of both spacecraft. This stabilizing behavior has been demonstrated through free-vibration simulations of closed-loop systems with nonzero initial conditions imposed on the spacecraft attitudes, as will be demonstrated in a forthcoming publication.

Future Considerations

The significant benefits that can be reaped from using a propulsion system that does not require expenditure of any propellant require further exploration. In this section, several concepts that warrant considerations are discussed.

The analysis in this paper uses the physical properties of materials at room temperature, except for the HTS wire, which was assumed to operate below its critical temperature at 77 K. The operation of the TPF interferometer at infrared wavelengths in free space requires the interferometer to be at temperatures of about 40 K. This is a suitable environment for superconducting. Also at this temperature, significant improvements in the material properties of conventional conductors, such as the conductivity of the coil, can be achieved.

This paper has assumed that the EM coil has been tightly wrapped around the spacecraft with structural connections of negligible mass. This is a convenient estimate because it puts a lower bound on the size of the EM coil and minimizes any additional structural mass. A more accurate structural model of the coil to spacecraft connections is necessary to determine what effect increasing the coil size has on the mass of the spacecraft.

Though not investigated, the spin-up mode of the interferometer must also be considered. Preliminary studies indicate that the TPF interferometer can be reasonably spun up from rest using just the EM dipoles and reaction wheels.[6] A separate publication is currently being developed to report on the viability of this spin-up mode and also determine the optimal method to spin up the interferometer.

The steady-state and spin-up operations for the EMFF interferometer are considered large motions for the spacecraft. To reject both external and internal disturbances, control strategies must be implemented. The control of other relative degrees of freedom between spacecraft (e.g., array shear, differential rotation, separation control, and differential roll about the baseline) can be investigated by considering small perturbations of the spacecraft. To gain authority over all relative degrees of freedom, quadrapole and electrostatic devices may need to be used.

This EMFF concept may also find application in rendezvous and docking, magnetic trapping of mirror facets into large segmented mirrors, etc. Additional applications include tension and shape control of membranes using EMFF spacecraft. Close proximity operations such as these are best suited for EMFF because the magnetic fields are stronger and avoiding plume impingement becomes more difficult at closer separations. Another consideration is the effect that such fields can have on spacecraft avionics. Shielding using materials such as mu-metal, analogous to a Faraday cage for electric fields, will help. Another option is to place small, oppositely poled dipoles (Helmholz coils) around the avionics bay to null the magnetic field locally near the avionics.

EMFF in low Earth orbit is also a possibility. EMFF can be used to counteract secular drift between spacecraft due to the Earth's J_2 perturbations.[7] It may also be feasible for reorienting or resizing arrays. Considerations now include operation in the presence of Earth's magnetic field, the strength needed to counteract differential drag and solar pressure, and interference with communication and radar payloads.

One could envision a space-based version of the Keck Observatory, where there is no need for a backbone truss to align the mirror segments. Only segment edge control is necessary and can be provided electromagnetically. Because of the soft interfaces, damaged facets can be removed, and additional facets can be launched and integrated into the array on an as-needed, as-afforded basis. The reduced contamination and lack of reliance on consumables make EMFF a technology warranting further exploration.

Summary

EMFF is feasible for missions such as NASA's TPF. In this study, electromagnets are shown to provide the centripetal acceleration necessary for array rotation. Furthermore, it does so with volume requirements, mass fractions, and power demands that are quite favorable when compared to thrusters.

When compared to propulsion systems, the EMFF concept is deemed to be the most attractive option especially when long mission lifetimes are considered. Such findings hold valid even for high specific impulse systems. The lack of propellant contamination and reliance on consumables further reinforces the viability of this EMFF concept.

In theory, the proposed EMFF interferometer can operate indefinitely, or at least until component failure because no nonrenewable resources (propellant) are used. System trades, as well as controllability studies and experimental validation, must be performed to determine if such an approach can be made to work.

References

[1]Beichman, C. A., Woolf, N. J., and Lindensmith, C. A. (eds.), "The Terrestrial Planet Finder (TPF): A NASA Origins Program to Search for Habitable Planets," Jet Propulsion Lab., Publ. 99-003, California Inst. of Technology, Pasadena, CA, May 1999.

[2]Larson, W., and Wertz, J., *Space Mission Analysis and Design*, 2nd ed., Microcosm and Kluwer Academic, Norwell, MA, 1998, Chap. 11.

[3]"Optimization Toolbox For Use with MATLAB—User's Guide," Ver. 2, Mathworks, Natick, MA, 2001.

[4]Reichbach, J., Sedwick, R. J., and Martinez-Sanchez, M., "Micropropulsion System Selection for Precision Formation Flying Satellites," Space Engineering Research Center, Rept. 1-01, Massachusetts Inst. of Technology, Cambridge, MA, Jan. 2001.

[5]Elias, L. M., Kong, E. M., and Miller, D. W., "An Investigation of Electromagnetic Control for Formation Flight Applications," Society of Photo-Optical Instrumentation Engineers Highly Innovative Space Telescope Concepts Conf., Paper SPIE 4849-24, Aug. 2002.

[6]Sedwick, R. J., and Schweighart, S. A., "Propellantless Spin-Up and Reorientation of Tethered or Electromagnetically Coupled Spacecraft," Society of Photo-Optical Instrumentation Engineers Highly Innovative Space Telescope Concepts Conf., Paper SPIE 4849-26, Aug. 2002.

[7]Schweighart, S. A., and Sedwick, R. J., "High-Fidelity Linearized J2 Model for Satellite Formation Flying," *Journal of Guidance Control, and Dynamics*, Vol. 25, No. 5, 2002, pp. 1073–1080.

A. Ketsdever
Associate Editor